The Non-universality of the Low-mass End of the IMF is Robust against the Choice of SSP Model

Spiniello, C.; Trager, S. C.; Koopmans, L. V. E.

Published in:
The Astrophysical Journal

DOI:
10.1088/0004-637X/803/2/87

Publication date:
2015

The Astrophysical Journal, 803:87 (15pp), 2015 April 20 doi:10.1088/0004-637X/803/2/87

THE NON-UNIVERSALITY OF THE LOW-MASS END OF THE IMF IS ROBUST AGAINST THE CHOICE OF SSP MODEL

C. Spiniello[1], S. C. Trager[2], and L. V. E. Koopmans[2]
[1] Max-Planck Institute for Astrophysics, Karl-Schwarzschild-Strasse 1, D-81740 Garching, Germany
[2] Kapteyn Astronomical Institute, University of Groningen, P.O. Box 800, 9700 AV Groningen, The Netherlands
Received 2014 June 27; accepted 2015 February 13; published 2015 April 21

ABSTRACT

We perform a direct comparison of two state-of-the art single stellar population (SSP) models that have been used to demonstrate the non-universality of the low-mass end of the initial mass function (IMF) slope. The two public versions of the SSP models are restricted to either solar abundance patterns or solar metallicity, too restrictive if one aims to disentangle elemental enhancements, metallicity changes, and IMF variations in massive early-type galaxies (ETGs) with star formation histories different from those in the solar neighborhood. We define response functions (to metallicity and α-abundance) to extend the parameter space for each set of models. We compare these extended models with a sample of Sloan Digital Sky Survey (SDSS) ETG spectra with varying velocity dispersions. We measure equivalent widths of optical IMF-sensitive stellar features to examine the effect of the underlying model assumptions and ingredients, such as stellar libraries or isochrones, on the inference of the IMF slope down to $\sim 0.1\,M_{\odot}$. We demonstrate that the steepening of the low-mass end of the IMF based on a non-degenerate set of spectroscopic optical indicators is robust against the choice of the stellar population model. Although the models agree in a relative sense (i.e., both imply more bottom-heavy IMFs for more massive systems), we find non-negligible differences in the absolute values of the IMF slope inferred at each velocity dispersion by using the two different models. In particular, we find large inconsistencies in the quantitative predictions of the IMF slope variations and abundance patterns when sodium lines are used. We investigate the possible reasons for these inconsistencies.

Key words: dark matter – galaxies: elliptical and lenticular, cD – galaxies: evolution – galaxies: kinematics and dynamics – galaxies: structure

1. INTRODUCTION

Evolutionary population synthesis is a proven technique to quantitatively study the luminous stellar content of unresolved stellar populations, first implemented by Tinsley (Tinsley 1968, 1972; Tinsley & Gunn 1976). Using stellar evolution theory and stellar spectra it is possible to derive relevant stellar population parameters such as age, metallicity, the shape of the stellar initial mass function (IMF), element abundance, and the physical state and quantity of dust in galaxies (e.g., Conroy 2013).

Many of the fundamental properties of unresolved stellar populations are encoded in their spectral energy distributions (SEDs), and a significant effort has been invested over the last 30 yr to construct detailed stellar population synthesis models to extract information from the SEDs of galaxies (e.g., Buzzoni 1989; Bruzual & Charlot 1993, 2003; Bressan et al. 1994; Worthey 1994; Leitherer et al. 1999; Maraston 2005). All stellar population synthesis models are based primarily on three ingredients, which determine the quality of the predictions: (1) a prescription for the IMF, (2) a set of stellar evolutionary prescriptions, and (3) one or more stellar spectral libraries, either theoretical or empirical.

Historically the IMF has been considered universal and the same as that of the Milky Way (e.g., Bell & de Jong 2001; Kroupa 2001; Chabrier 2003; Bastian et al. 2010). However, in recent years increasingly more observational and theoretical evidence based on different and independent methods supports the idea of a non-universal low-mass end of the IMF. Gravitational lensing combined with dynamics modeling (e.g., Auger et al. 2010; Treu et al. 2010) and stellar population modeling (Spiniello et al. 2012, 2014, hereafter S12 and S14, respectively), spectroscopic stellar population analysis alone (e.g., Conroy & van Dokkum 2012b; La Barbera et al. 2013), and spatially resolved kinematics and dynamics (Cappellari et al. 2012; Läsker et al. 2013; Tortora et al. 2013) have all shown that the slope of the low-mass end of the IMF steepens with galaxy mass.

Recently, two new single stellar population (SSP) models have been developed with the specific purpose of studying metal-rich, old stellar populations: Conroy & van Dokkum (2012a, hereafter CvD12) and Vazdekis et al. (2012, hereafter MIUSCAT). The aim of this paper is to compare the models to understand whether or not the recent suggestions that the IMF steepens with galaxy velocity dispersion (S12, S14, Conroy & van Dokkum 2012b; Ferreras et al. 2013; La Barbera et al. 2013) merely arises from a misunderstanding of their main ingredients. When using these SSP models to infer the stellar populations from unresolved spectra of old, evolved galaxies, it is essential to demonstrate that the conclusions about and predictions for the galaxy parameters do not depend on the assumptions of the model itself. As we demonstrate below, the evidence for a steepening of the low-mass IMF based on line indices is indeed robust, but care must be taken in using some line indices and a wide enough parameter space must be explored to break degeneracies between metallicity, age, elemental abundance, and IMF variations.

The paper is organized as follows. In Section 2 we give a brief introduction of the two sets of models and highlight their similarities and differences. In Section 3 we compare each model independently with SDSS galaxies. In Section 4 we derive the IMF–$\sigma^{\star}$ relation using a set of IMF-sensitive features for which the models give similar prediction. In Section 5 we

discuss our findings and present our conclusions. Finally, in Appendix A we perform a direct comparison of the behavior of single absorption-line indices for both models, and we focus on the impact of the different model ingredients and assumptions on the inference of the low-mass end of the IMF slope.

2. SIMPLE STELLAR POPULATION MODELS

In this section we provide a brief introduction of the two sets of SSP models. We describe the main ingredients and the space of stellar parameters that are explored before proceeding in Section 3 to compare each model with data on massive early-type galaxies (ETGs).

A more detailed comparison between the different underlying assumptions and ingredients of the two SSP models is presented in Appendix A. There we analyze the effect of the different isochrones, stellar libraries, and different approaches in dealing with metallicity on the inference about the low-mass end of the IMF slope.

2.1. Conroy and van Dokkum SSP Models

CvD12 presented new SSP models with variable abundance patterns and stellar IMFs, that are models suitable to study spectra of galaxies with ages $\geqslant$3 Gyr.[3] These models explore variations in [α/Fe], but all of them have solar total metallicity, even when synthesizing models with different abundance patterns. They use a combination of three different isochrones to explore the separate phases of stellar evolution: (i) the Dartmouth isochrones (Dotter et al. 2008) for the main sequence and the red giant branch (RGB), (ii) the Padova isochrones (Marigo et al. 2008) to describe AGB evolution and the horizontal branch (HB), (iii) and the Lyon isochrones (Chabrier & Baraffe 1997; Baraffe et al. 1998) for stars with masses $M \leqslant 0.2\,M_{\odot}$. The wavelength interval covered by the final fiducial model is $0.35\ \mu\mathrm{m} < \lambda < 2.4\ \mu\mathrm{m}$ at a resolution of $R \simeq 2000$. The CvD12 models use two separate empirical stellar libraries: the MILES library over the wavelength range $0.35\ \mu\mathrm{m} < \lambda < 0.74\ \mu\mathrm{m}$ (Sánchez-Blázquez et al. 2006) and the IRTF library of cool stars over the wavelength range $0.81\ \mu\mathrm{m} < \lambda < 2.4\ \mu\mathrm{m}$ (Cushing et al. 2005), plus synthetic stellar spectra to cover the gap between these two models and to investigate spectral variations due to changes in individual elemental abundances. In the version of the code that we examined, the model allows for variations in the elements C, N, Na, Mg, Si, Ca, Ti, Cr, Mn, Fe, O, Ne, and S. We use here a more recent version of the models, presented in Conroy et al. (2014), that uses M dwarf templates from SDSS (Bochanski et al. 2007) to supplement the (very small) number of dM stars present in the MILES library.

With the isochrones and stellar libraries described above, CvD12 constructed integrated light spectra via the equation

$$f(\lambda) = \int_{m_l}^{m_u(t)} s(\lambda, m)\phi(m)dm, \qquad (1)$$

where the integral over stellar masses ranges from the hydrogen burning limit (assumed to be $m_l = 0.08\,M_{\odot}$) to the most massive star alive at time t. In Equation (1), f is the integrated spectrum, s is the spectrum of a single star, and $\phi(m) = dN/dm$ is the IMF. All stars in the population are assumed to have the same metallicity and abundance pattern. CvD12 explore variations in age between 3 and 13.5 Gyr with four different single-slope IMFs—a Chabrier (2003) Milky Way-like IMF with a slope of $x = 1.8$, hereafter referred to as the "MW IMF," a Salpeter IMF ($x = 2.3$), and two bottom-heavy IMFs with slopes of $x = 3.0$ and $x = 3.5$—and different α-enhancement and individual element abundances.

2.2. The MIUSCAT SSP Models

The MIUSCAT models are an extension of the stellar population synthesis models based on the MILES (Sánchez-Blázquez et al. 2006) and CaT (Cenarro et al. 2001) empirical stellar spectral libraries to cover the spectral range $0.346\ \mu\mathrm{m} < \lambda < 0.947\ \mu\mathrm{m}$. Moreover, the spectral coverage is extended to the blue and red wavelengths with the Indo-U.S. library (Valdes et al. 2004). In order to determine which stars to include in the synthesis, they use the solar-scaled theoretical isochrones of Girardi et al. (2000), which cover a wide range of ages, and six metallicity bins. The Girardi isochrones include a simple synthetic prescription that incorporates the thermally pulsing AGB regime (Bertelli et al. 1994). Moreover, an improved version of the equation of state, new opacities from Alexander & Ferguson (1994), and a convective overshoot scheme have been added to the models to improve the physics of these latest stages of stellar evolution. The stars are then attached to the isochrones according to their number per mass bin, predicted from the adopted IMF. Different IMF shapes are considered: the unimodal and bimodal power-law IMFs defined in Vazdekis et al. (1996), and the multi-part power-law IMFs of Kroupa (2001). The Salpeter (1955) IMF is represented by the unimodal case with slope $\Gamma = x - 1 = 1.3$. Here we restrict to the unimodal power-law IMFs to perform a fair comparison with CvD12. We use the Kroupa (2001) "universal" IMF to represent a Milky Way-like IMF for the MIUSCAT models, referred to hereafter as the "MW IMF." We caution the reader that this IMF is not exactly the same as the "MW IMF" used in the CvD12 models (single power-law with a slope $x = 1.8$ that gives a mass-to-light ratio (M/L) similar to the one obtained with a standard Chabrier), but should be close given the similar shapes and normalization (see, e.g., Chabrier 2005).

The lower stellar mass limit (cutoff mass) assumed by the MIUSCAT models, given the Girardi et al. (2000) isochrones, is $M_{\mathrm{low}} = 0.15\,M_{\odot}$, and is slightly higher than that used in CvD12. From a spectroscopic point of view, the adoption of a slightly higher value of M_{low} does not have a large impact on the line-strength measurements, although it can have a visible contribution for some spectral features (see Figure 15 in Conroy & van Dokkum 2012a). However, one must keep in mind that even though stars below $\sim$0.1 $M_{\odot}$ are almost invisible in current spectral lines, they can contribute substantially to the total stellar mass and number of stars for any standard IMF. As discussed in Barnabè et al. (2013), the value of M_{low} is an essential parameter when determining $\Upsilon_{\star}$ from stellar population codes.

2.3. Extending the Parameter Space of the Models

A significant difference between the two sets of models is their approach in dealing with metallicity and [α/Fe]. The CvD12 models use solar metallicity isochrones, even when synthesizing models with different abundance patterns. The total metallicity Z varies from model to model because the

[3] A more recent version of the SSP presented in Choi et al. (2014) is capable of fitting populations as young as 1 Gyr.

abundance variations of single elements are implemented at a fixed [Fe/H]. The MIUSCAT models, on the other hand, do not allow the relative abundance of the α-elements to change and are therefore restricted to the solar abundance pattern, although there are models with different total metallicities. Each MIUSCAT SSP has a fixed total metallicity and MIUSCAT has six metallicity values in total ($Z = 0.0004$, 0.001, 0.004, 0.008, 0.019, and 0.03, corresponding to $[M/H] = -1.71$, −1.31, −0.71, −0.40, 0.0, +0.22).

Therefore, the only direct comparison possible between the public versions of the models is at solar metallicity and solar [α/Fe]. This is restrictive if one aims to disentangle elemental enhancements, metallicity changes, and IMF variations. This is especially true for very massive ETGs, which are known to be α-enriched and to have slightly super-solar metallicity, due to star formation histories different from the solar neighborhood (e.g., Peterson 1976; Peletier 1989; Worthey 1992; Trager et al. 2000b; Arrigoni et al. 2010).

To resolve this, at least on a qualitative level, we extend the parameter space from each set of models in the following ways. We take the ratio between two spectra of MIUSCAT models with the same age and IMF slope but different total Z. In this way we isolate the effect of changing the total metallicity from the effect of changing other stellar population parameters, i.e., we construct a metallicity-response function for each given age and IMF slope. We then multiply this response function with the spectrum of a CvD12 model with the same age and IMF to build a new model (SSP) that extrapolates the latter model to a new part of the parameter space (i.e., covering super-solar Z):

$$\Delta Z(\tau, x) = \frac{\mathrm{MIU}(\tau, x, Z)}{\mathrm{MIU}\left(\tau, x, Z_{\odot}\right)} \quad (2)$$

$$\mathrm{CvD12}_{\mathrm{ext}}(\tau, x, Z) \equiv \mathrm{CvD12}(\tau, x) \times \Delta Z(\tau, x) \quad (3)$$

where τ is the age of the stellar population and $Z > Z_{\odot}$ is the super-solar metallicity value explored by the MIUSCAT models ($Z = 0.03$, corresponding to $[M/H] = +0.22$).

In the same way, we use CvD12 models at a fixed age and IMF slope to build an [α/Fe]-response function that we then multiply with MIUSCAT models to build models with super-solar [α/Fe] abundances

$$\Delta[\alpha/\mathrm{Fe}](\tau, x) = \frac{\mathrm{CvD12}(\tau, x, [\alpha/\mathrm{Fe}])}{\mathrm{CvD12}\left(\mathrm{age}, x, [\alpha/\mathrm{Fe}]_{\odot}\right)} \quad (4)$$

$$\mathrm{MIU}_{\mathrm{ext}}(\tau, x, [\alpha/\mathrm{Fe}]) \equiv \mathrm{MIU}(\tau, x) \times \Delta[\alpha/\mathrm{Fe}](\tau, x), \quad (5)$$

where the super-solar [α/Fe] values explored by the CvD12 models are 0.2, 0.3, and 0.4.

These modified SSP models combine the flexibility of both the MIUSCAT and CvD12 models to predict spectra in a part of parameter space that neither of them reaches separately. Allowing for variation in age, metallicity, and [α/Fe]—i.e., selecting IMF-dependent features that are age- and metallicity-independent and combining them with indices that depend mainly on age or mainly on element abundance—is important to break the age - metallicity - IMF degeneracy when using SSP models to infer the stellar populations from unresolved galaxy spectra.

However, it is important to clarify that the model extension performed above has to be interpreted as a first order approximation meant to demonstrate that the IMF–$\sigma_{\star}$ relation is a robust result, independent of the choice of SSP model. In fact, the two SSP models differ in many of their main ingredients and construction methods such as the isochrones, the interpolation scheme, or the conversion of the theoretical parameters of the isochrones to observational quantities. Nevertheless we show in this paper that the combined models are very useful to demonstrate the robustness of the results on the IMF variation obtained with the CvD12 or MIUSCAT models separately.

In Figure 1 we plot spectra of a $\mathrm{CvD12}_{\mathrm{ext}}$ SSP model (black) and an $\mathrm{MIU}_{\mathrm{ext}}$ SSP model (red) with the same age (12.5 Gyr), super-solar metallicity ($Z = +0.03$), super-solar [α/Fe] (= +0.2), and IMF (MW in the upper panels and $x = 3.0$ in the lower panels) to verify that the extrapolated versions of the CvD12 and MIUSCAT models agree for the same stellar population parameters, validating our methodology.

Spectra with an MW-like IMF typically agree within $\leqslant 1\%$, demonstrating that our approach of extrapolating one model using a response function obtained from the other provides mutually consistent answers. However, some differences are visible in the case of a bottom-heavy IMF ($x = 3.0$), especially for the NaD and TiO_2 absorption features. This implies that the two sets of models give different predictions on the variations of the index strength with IMF slope if these indices are used. In the following we demonstrate that this difference is caused by the different ingredients and assumptions of the two models. In particular, we show that part, but not all, of the difference is due to the different sets of isochrones used in the two models. Another source of this difference is from the different ways in which CvD12 and MIUSCAT attach stars to the isochrones (see Appendix A for more details). Despite these differences, we show in this paper that both models predict a non-universality of the low-mass end of the IMF, which steepens with the stellar velocity dispersion.

3. COMPARISON WITH DATA

We now compare the extended versions of the CvD12 and MIUSCAT models with data on ETGs and show that the non-universality of the low-mass end of the IMF holds and appears to be robust against the choice of SSP model in a relative sense. We use a sample of SDSS spectra that has been selected and extensively described in S12 and S14. The spectra were averaged ("stacked") in five velocity dispersion bins spread over 150–310 km s^{-1} to increase the final signal-to-noise ratio in each bin. Below 150 km s^{-1} contamination from spiral galaxies becomes larger and emission lines affect our results considerably. We refer to S14 for further details.

We perform line strength measurements following the approach presented in Trager et al. (2008) and using their Python implementation of the algorithm, SPINDEX2. We measure the standard Lick indices Hβ, Mgb, Fe5270, Fe5335, NaD, and TiO_2 using the definitions of Trager et al. (1998), the broadly used [MgFe] combination,[4] and the IMF-sensitive set of optical indicators described in S14. Finally, we use the modified NaI index defined in Spiniello et al. (2012) and the CaT index (Cenarro et al. 2001). We measure indices in the wavelength range 4000–8500 Å. We are aware that for wavelengths redder than ∼7500 Å the two models make use of different stellar libraries (see Appendix A for more details). All the galaxy and model spectra are convolved to a final velocity dispersion of $\sigma = 350$ km s^{-1} to correct for kinematic

[4] $[\mathrm{MgFe}] = \sqrt{(\mathrm{Fe5270} + \mathrm{Fe5335})/2 \times \mathrm{Mgb}}$, González (1993).

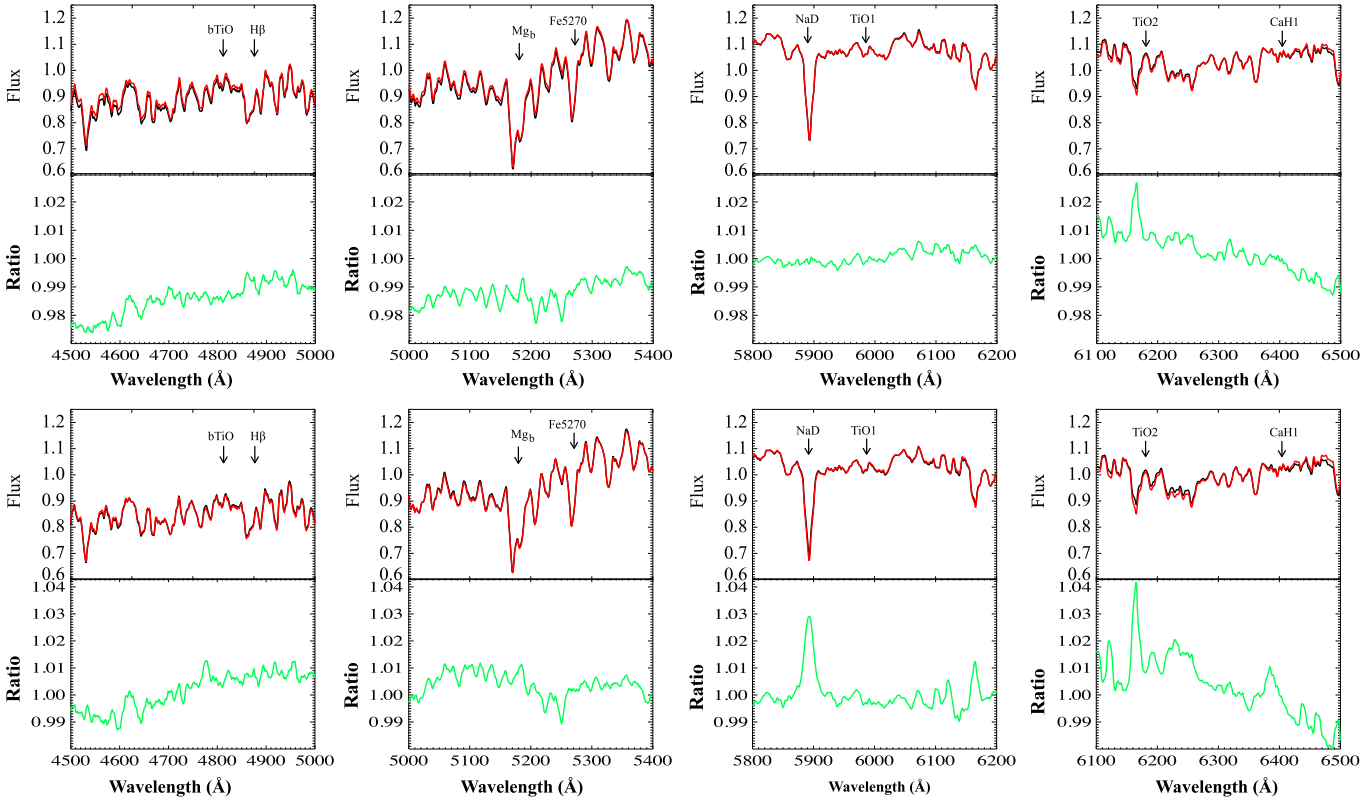

Figure 1. Zoom-in of different regions of a $\mathrm{CvD12_{ext}}$ SSP model spectrum (in black) and an $\mathrm{MIU_{ext}}$ SSP model spectrum (in red) for an MW IMF (top panels) and a bottom-heavy IMF ($x = 3.0$, bottom panels). Both models have the same age (12.5 Gyr), super-solar metallicity ($Z = 0.03$), and super-solar [α/Fe] ([α/Fe] = +0.2). The spectra have the same resolution (FHWM = 2.51 Å) and are plotted in units of normalized flux. Some absorption lines are highlighted in the plots and the ratios between the spectra are shown in the lower green panels. The spectra obtained via the response functions are very similar, especially in the case of an MW-like IMF (1% agreement), demonstrating the validity of the extrapolation approach. Some differences are visible for the spectra having a bottom-heavy IMF. See the text for a detailed discussion.

broadening before measuring line strength. Indices in both the galaxies and the two sets of model spectra are measured with the same definitions and methods. We do not place our indices on the zero point system of the Lick indices, but instead present them as equivalent widths (EWs) in units of Å, except for the molecular TiO and CaH indices, which are given in magnitudes.

Figure 2 shows a zoom-in of the stacked ETGs and SSP model spectra in the bTiO, NaD, $\mathrm{TiO_1}$, and $\mathrm{TiO_2}$ regions, with the index bandpass as well as the blue and red pseudo-continua bands shown as boxes. A clear increase of the line strengths of all these features are visible in all panels, although in some cases (e.g., NaD) the data show a somewhat stronger variation due to the fact that these indices are not only gravity sensitive, but also depend on individual elemental abundances and possibly age. For instance, for the CvD12 models, which allow variation of the Ti and Na abundance pattern, we investigate whether a non-solar [Ti/Fe] abundance (left and right panels, second row) or a non-solar [Na/Fe] abundance (middle panel, second row) could significantly vary the indices strength and explain the variation seen in the data. It is clear that the variation due to IMF can be mimicked by non-solar abundance. We therefore stress that the use of many indicators, arising from different features, is crucial to break such degeneracies (S14). In particular, in the case of the NaD index, the variation of the NaD EWs in the CvD12 models due to a non-solar [Na/Fe] abundance is larger than the variation due to the IMF slope. The larger variation of NaD EWs due to a non-solar [Na/Fe] abundance seems to be in better agreement with the variation observed for SDSS galaxies. We investigate this further in Appendix B; however we caution the reader that this is a model-dependent result.

In Figures 3 and 4 we present index–index plots of the IMF-sensitive features for the two extended sets of models and the stacked SDSS galaxies. Remarkably, the massive galaxies better match SSP models with steeper IMF slopes independently of the considered set of models in all panels. Index–index plots are a useful tool to give a qualitative inference on the stellar population parameters, but a proper statistical analysis involving a wide range of spectral features is necessary to break degeneracies and quantitatively constrain age, metal abundance, and IMF slope, as we did in S14 via a χ^2 minimization routine (using CvD12). We restrict the comparison to a single SSP[5] age (12.5 ± 1 Gyr) with a varying IMF slope, metallicity, and [α/Fe] and focus only on features with a weak age sensitivity. In addition, we plot a younger MIUSCAT model (~9.0 Gyr) with solar α-abundance and metallicity to highlight the age effect on the line-index strength variations. We note that in S14 we find that all galaxies (with $\sigma \geqslant 150\,\mathrm{km\,s^{-1}}$) have old stellar populations (>9 Gyr).

[5] The two sets of models do not have a common old age: the oldest CvD12 models have ages of 11 and 13.5 Gyr respectively; the oldest MIUSCAT models have ages of 12.5 and 14.1 Gyr. Therefore we interpolated the CvD12 models to create 12.5 Gyr models to eliminate most of the residuals arising from age differences.

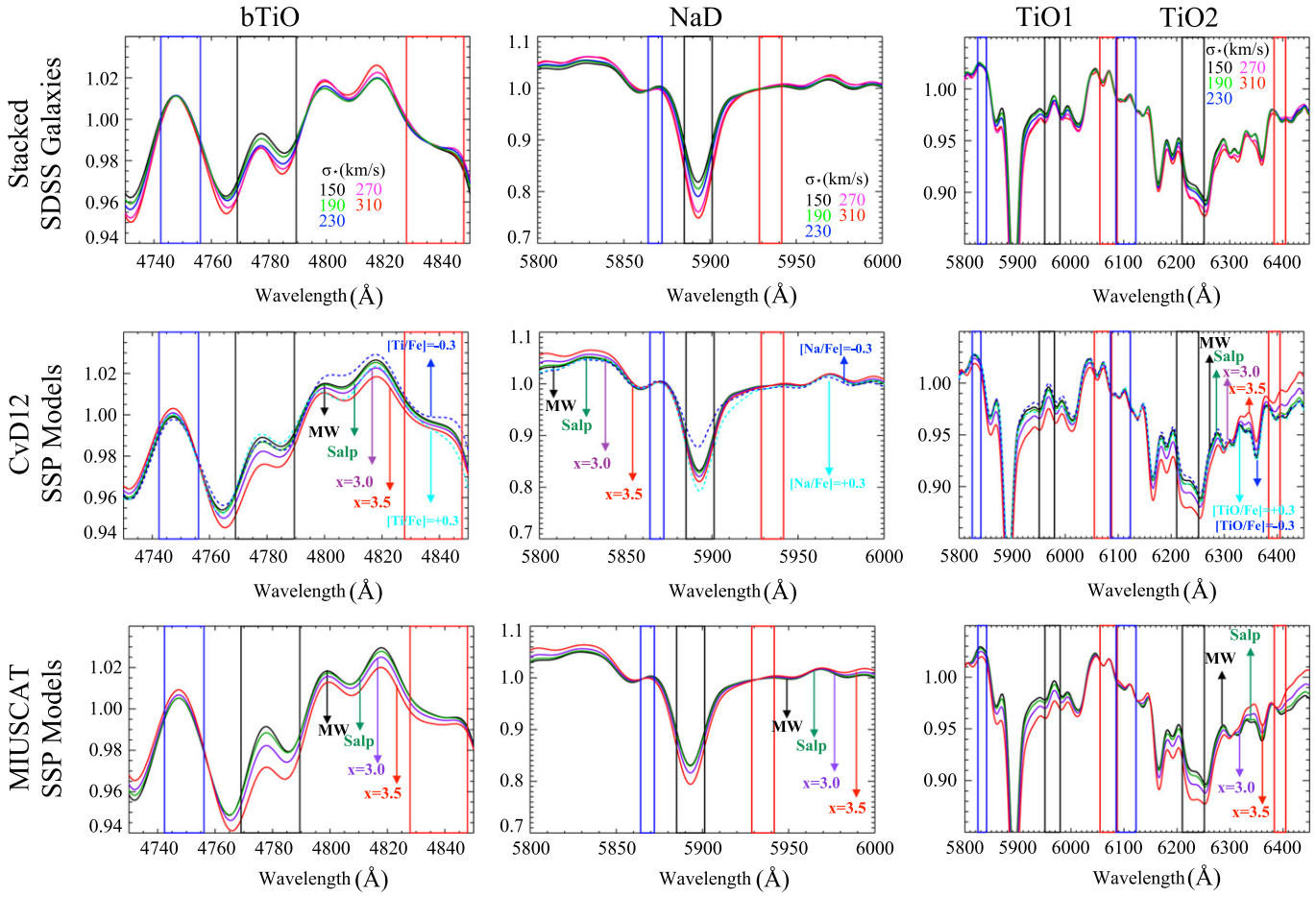

Figure 2. Galaxy (top row) and SSP model (middle and bottom rows) spectra in the regions of the bTiO, NaD, TiO_1, and TiO_2 absorption features. A clear trend of increasing EWs is visible in both the data and models, although the data show a stronger variation (see the text). The bandpasses of the indices, as well as the blue and red pseudo-continua, are shown as boxes in the plots. Top row: spectra of SDSS galaxies stacked in different velocity dispersion bins over the range of 150–310 km s^{-1}. Middle row: CvD12 SSP models with an age of 13.5 Gyr and solar [α/Fe], but with different IMF slopes from MW-like to very bottom-heavy ($x = 3.5$). Dotted lines show models with MW-like IMFs and different [Ti/Fe] or [Na/Fe] abundances. Bottom row: MIUSCAT SSP models with an age of 14.2 Gyr and solar metallicity, but with different IMF slopes from MW-like to an extremely bottom-heavy IMF with a slope of $x = 3.5$. All spectra are normalized to the central point of the blue and red pseudo-continuum bands.

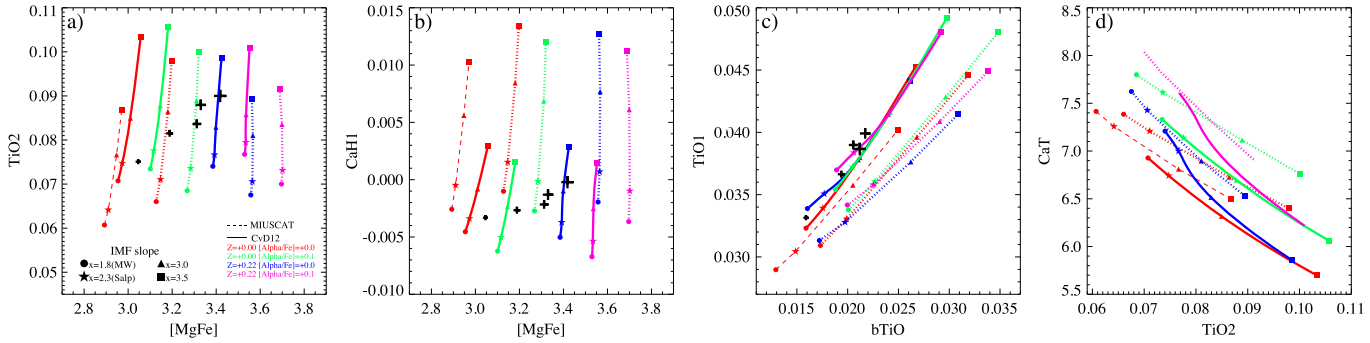

Figure 3. Index–index plots of some of the most prominent IMF-sensitive absorption features in the optical regime. Solid lines are CvD12 SSP models and dotted lines are MIUSCAT SSP models; both models have an age of 12.5 Gyr. The dashed line is a MIUSCAT model with an age of ∼9.0 Gyr. Red lines are SSP models with solar metallicity and solar [α/Fe], blue lines are SSP models with $Z = +0.22$ and solar [α/Fe], green lines are α-enhanced models with solar metallicity, and magenta lines are α-enhanced models with super-solar total metallicity. Symbols on each line represent different IMF slopes (see the legend). Black points with error bars are SDSS galaxies, stacked by velocity dispersions expressed in km s^{-1}. Larger symbols are galaxies with larger velocity dispersions. On a qualitative level, these diagrams show a good agreement of the two models with the galaxies for these indices: a clear trend of the low-mass slope of the IMF with galaxy mass is visible in both models, and the most massive ETGs require an IMF slope slightly steeper than Salpeter for both SSP models. However, absolute values of the inferred IMF slopes for each $\sigma_\star$ are different (see the text and Appendix A for more details). We remind the reader that TiO and CaH indices are given in magnitudes.

Very massive ETGs are known to be α-enriched and to have a slightly super-solar metallicity (see, e.g., Worthey 1994). Our aim here is to compare each set of models with the massive galaxy spectra bin and we therefore plot the models built using our response functions (see the previous section) with super-solar metallicity and super-solar [α/Fe].

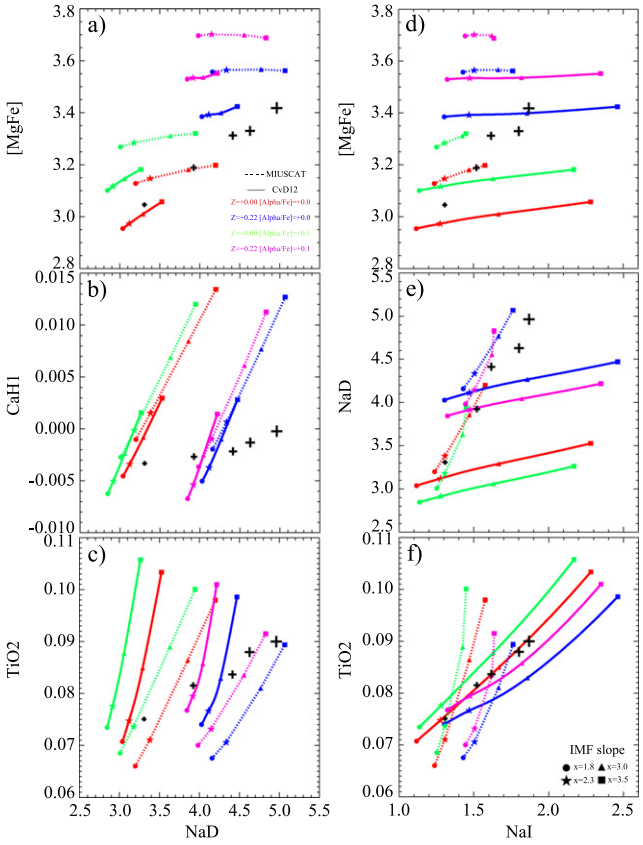

Figure 4. Index–index plots of blue sodium absorption feature NaD (left column, panels (a), (b), and (c)) and of red sodium absorption feature NaI (right column, panels (d), (e), and (f)) in the optical vs. other IMF-sensitive features. Lines and data points are the same as in Figure 3. Larger symbols are galaxies with larger velocity dispersions. In these plots the two sets of models give very different predictions for IMF variations. Panels (a), (c), and (e): MIUSCAT models with varying total metallicity match the data better at all $\sigma_\star$ than CvD12 models, but the most massive bin with $\langle\sigma\rangle = 310\,\mathrm{km\,s^{-1}}$ requires an extremely steep IMF with a slope of $x = 3.5$ (blue square), in disagreement with previous inferences based on lensing and stellar populations (Spiniello et al. 2012). Panel (b): none of the models match the data at any $\sigma_\star$. For each of these panels a sodium overabundance with [Na/Fe] = 0.3–0.5 (consistent with values found by O'Connell 1976; Peterson 1976; Carter et al. 1986; Alloin & Bica 1989; Worthey 1998; Worthey et al. 2011) in more massive galaxies can explain the disagreement between the models with the most massive galaxy bin. This is, however, a model-dependent result, obtained with CvD12. Panels (d) and (f): MIUSCAT SSP models do not match the index strengths of the very massive systems, while the CvD12 models with solar metallicity and varying IMF slopes do, without requiring an incredibly steep IMF slope for the most massive bin. As shown in Figure 9 and Table 2, NaI does not strongly depend on sodium abundance.

We limited ourselves to a unimodal IMF slope, the only choice for the CvD12 models, but we stress that it may not be possible to fully constrain the detailed functional form of the IMF (either unimodal or multi-segmented) using only index–index diagrams. For instance, although the *M*/*L*s obtained in S14 via line strength measurements assuming a unimodal IMF were consistent with the results of La Barbera et al. (2013), the inferred IMF slopes were not. These authors obtained steeper slopes when using a two-segmented (bimodal) IMF, yet found similarly good fits to the data using unimodal IMF slopes in their index–index plots. A note of caution should also be sounded concerning the fact that the two different SSP models adopt a different choice for $M_{\rm low}$, implying different results for the stellar *M*/*L*s (CvD12 use $0.08\,M_\odot$, while MIUSCAT adopt $0.10\,M_\odot$). We clarify that here (and in previous papers) the IMF–$\sigma^\star$ relation was obtained under the assumption of a fixed, universal lower cutoff mass ($0.10\,M_\odot$).

Figure 3 shows some of the IMF indicators in the optical that were shown to robustly break degeneracies in the SSP models between age, metallicity, abundance pattern, and IMF slope in S14. For both models this set of indicators clearly shows a steepening of the IMF slope with stellar velocity dispersion (galaxy mass), although zero point shifts and differences in the absolute values of the IMF slopes are visible (see Appendix A). The models imply an MW-like IMF for the least-massive galaxies ($\langle\sigma_\star\rangle = 150\,\mathrm{km\,s^{-1}}$), a Salpeter IMF for the intermediate-mass ETGs, and possibly a bottom-heavy IMF (with $x \sim 3$) for the most massive galaxies. This result is fully consistent with the more detailed analysis performed in S12, S14, and in completely independent studies (e.g., La Barbera et al. 2013) but done here using both the CvD12 and MIUSCAT models in a consistent way.

Panels (a), (c), and (d) of Figure 3 show a fair agreement between the two sets of models and the galaxies for old stellar populations, although some differences still remain. The [MgFe]–TiO_2 diagram (panel (a)) suggests that more massive galaxies require super-solar metallicity and possibly also super-solar [α/Fe]. The same is also visible in panel (b), but in this diagram the differences in the absolute IMF values are extreme. In fact, CaH_1 variations with IMF slope predicted from the two sets of models are extremely different, and an offset for this index is also present. In panels (c) and (d) the dependencies on Z and [α/Fe] are minimal and somehow degenerate with IMF slope. Here the models give similar predictions for the steepening of the IMF slope, but an offset between MIUSCAT and CvD12 models with the same parameters is found. We investigated the possible reasons for this offset in Appendix A and found that the different isochrones used by the two models play a non-negligible role for most of the indicators, but do not solve the problem for the TiO_2 index. We believe that this difference is primarily due to the different methods used in the CvD12 and MIUSCAT models to attach stars to the isochrones at low mass.

Panel (d) confirms the previously known fact that the CaT index is almost metallicity independent,[6] as is visible from the MIUSCAT models, while it strengthens with increasing [α/Fe]. The two SSP models use different libraries in the CaT wavelength range, but still lead to the same prediction for the IMF variation. We therefore conclude that the use of different libraries is not responsible for the large disagreement visible when sodium lines are used.

Finally, we note that the zeropoint shift cannot be explained by allowing for an age offset between the two sets of models. A MIUSCAT model with age ~9 Gyrs (red, dashed line in Figure 3) and with an MW-like IMF predicts a [MgFe] strength very similar to that predicted by CvD12 with the same IMF, but ~4 Gyr older. However, the EWs predicted by these two models with different ages for the bTiO and the TiO_2 indices are in much worse agreement with respect to those predicted from models with the same age.

3.1. The Sodium Features

In Figure 4 we plot the two sodium absorption features in the optical (the blue NaD index at $\lambda \sim 5900$ Å on the left column

[6] This is true when $[Z/H] \geqslant -0.5$, which is the case for the giant ETGs considered here.

and the redder NaI doublet at $\lambda \sim 8190$ Å on the right) against the IMF-sensitive features previously introduced. In all cases the two models have very different behavior and in similar cases they fail to match the data at all velocity dispersions. Specifically, the CvD12 models with a solar abundance pattern only match the low-mass systems in all panels with NaD ((a), (b), and (c)).[7] The MIUSCAT models better match the data at all velocity dispersions, but do not predict the same IMF slope for the same velocity dispersion bin in each panel. In panel (b) the IMF slope for the most massive bin is close to a Salpeter IMF, whereas in panels (a) and (c) MIUSCAT predicts extremely bottom-heavy IMF slopes, steeper than those inferred from other absorption-line indices of Figure 3.[8] These trends also violate lensing and dynamical constraints (Treu et al. 2010; Spiniello et al. 2011, 2012; Barnabè et al. 2013).

Given this situation, further investigation into the different behaviors of the sodium indices in the two SSP models is necessary. We show in Appendix B that the NaD index is much more sensitive to [Na/Fe] abundance than to IMF slope variation in the CvD12 models. Moreover, if one assumes a relation between [Na/Fe] and $\sigma_{\star,}$ in the sense that more massive galaxies are Na-enhanced, then the CvD12 models match the data in all velocity bins. Although a non-solar [Na/Fe] abundance for more massive galaxies has been reported in the literature (e.g., Jeong et al. 2013), we stress that this result is model-dependent and should therefore be taken with some caution.

We emphasize that NaD lies in a part of the spectrum for which the two sets of models use the same stellar library, while NaI lies in the redder part where the models make use of two different stellar libraries. Therefore the large difference in the NaD behavior cannot be attributed to the different stars used when constructing the SSP models and is indeed likely due to a varying [Na/Fe] abundance.

In conclusion, we argue that the observed trends of NaD and NaI are unlikely to be completely due to a variation in the IMF as a function of velocity dispersion, but may (in part) be caused by Na enhancement in massive galaxies.

4. IMF SLOPE VERSUS VELOCITY DISPERSION

We now give a more quantitative expression for the variation of the IMF slope with stellar velocity dispersion, following the same approach as in S14. In particular, we compare each stacked SDSS spectrum with the grids of interpolated and extended SSPs. The models cover a large range of ages (log (age) = [0.8–1.15] Gyr, with a step of 0.01 Gyr), [α/Fe] (between −0.2 and +0.4 dex, with a step of 0.05 dex), total metallicity ([*M*/*H*] between −0.4 and +0.22), and IMF slope ($x = [1.8–3.5]$, with a step of 0.1). The following indices allow us to constrain the IMF slope and concurrently break the degeneracies between age, abundance ratio, and total metallicity: Hβ, Mgb, Fe5270, Fe5335, bTiO, aTiO, TiO_1, TiO_2, CaH_1, CaT1, CaT2, and CaT3. For each velocity dispersion bin and SSP model we compute the χ^2 and then obtain the best-fitting IMF slope and its uncertainty, marginalizing over age, metallicity, and [α/Fe]c while assuming flat priors on all parameters.

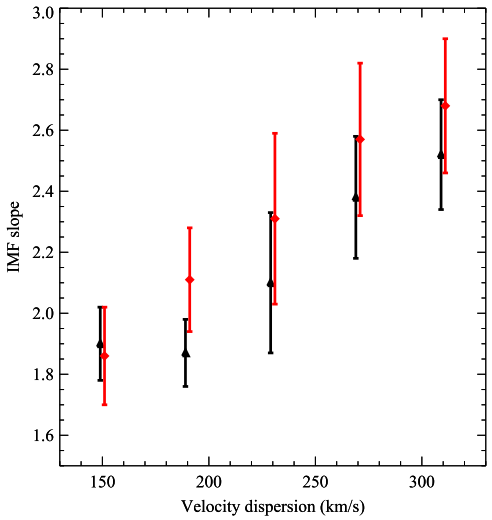

Figure 5. Variation of the IMF slope as a function of stellar velocity dispersion predicted from the CvD12 SSP models (black) and the MIUSCAT SSP models (red). Points are SDSS ETGs stacked by velocity dispersion. A fair agreement (within 1σ error) is found between the IMF slopes predicted from the two sets of models and also with previous work (e.g., S14, La Barbera et al. 2013).

Unfortunately we cannot investigate the effect of changing the effective temperature of the isochrones, as we did in S14, because MIUSCAT models with $\Delta T_{\rm eff} \neq 0$ are not publicly available. However, we perform a test for CvD12 to provide a comparison to the non-extended CvD-based fits performed in S14. We repeat the χ^2 analysis with the same set of indicators for CvD12 SSPs with varying age, [α/Fe], [*M*/*H*], IMF, and $\Delta T_{\rm eff}$ (between −200 and +200 K, with a step of 50 K). We find that age, [α/Fe], and IMF constraints are almost independent of $\Delta T_{\rm eff}$ (i.e., results obtained with models with $\Delta T_{\rm eff} = 0$ are consistent with those obtained with $\Delta T_{\rm eff}$ as a free parameter), whereas inferred total metallicities are systematically lower when $\Delta T_{\rm eff}$ is allowed to change. We note that compared to S14, where a trend of changing the temperature scale of the giant stars with galaxy mass was inferred using models with solar metallicity (more massive galaxies seemed to have a colder population), here all SDSS bins are consistent with $\Delta T_{\rm eff} = -50 \pm 30$.

We plot the IMF–σ relation in Figure 5 for both models (CvD12 in black, MIUSCAT in red). A remarkable agreement is found between the IMF slope inferred on each SDSS spectrum from the two different set of models, although MIUSCAT predicts on average slightly steeper (by about +0.2) IMF slopes for the more massive bins. The result of our analysis confirms the findings of S14 and shows that the non-universality of the low-mass end of the IMF is a robust and model independent result.

5. CONCLUSIONS

In this paper we have compared the two state-of-the-art SSP models by Conroy & van Dokkum (2012a) and Vazdekis et al. (2012), specifically constructed for the purpose of studying the stellar population of old, metal-rich systems with SDSS ETGs with increasing stellar velocity dispersions from 150 to 310 km s^{-1}. We show that both models predict a non-universal

[7] We confirm here the finding of S12 that for the CvD12 models the NaD indices and their trends with stellar mass remain unexplained, at least for the more massive systems with $\sigma \geqslant 200$ km s^{-1}, using models with a solar abundance pattern.

[8] The same result was obtained for CvD12 models in S14. In S14 we show that the quantitative relation inferred between the IMF slope and velocity dispersion, including the NaD index, is systematically different than the relation inferred from any other combination of the IMF-sensitive spectral indices mentioned above.

low-mass end of the IMF slope that steepens with increasing galaxy mass.

To overcome the limits of each model, we have extended their parameter spaces by calculating two independent response functions (one based on metallicity from MIUSCAT and another based on [α/Fe] from CvD12) to better study massive elliptical galaxies, which are overabundant in α-elements relative to the Sun and metal-rich (e.g., Peterson 1976; Peletier 1989; Worthey et al. 1992; Trager et al. 2000a; Arrigoni et al. 2010).

Although this model extension is not fully consistent because of the different ingredients and assumptions of the SSP models, we show that it is very useful to demonstrate the robustness of the results on the IMF variation obtained with CvD12 or MIUSCAT models separately. Moreover, using these two response functions, we find remarkable agreement between these two SSP models outside their original parameter space when the Na lines are excluded, something that a priori might not have been expected.

Our main conclusions are as follows.

1. Independently of the chosen stellar population model, the non-universality of the low-mass end of the IMF is a robust result. A clear trend of the IMF slope with galaxy velocity dispersion is found, under the assumption of a universal $M_{\rm low}$. This result is consistent with other published works (Treu et al. 2010; Cappellari et al. 2012; Spiniello et al. 2012; La Barbera et al. 2013; Tortora et al. 2013, S14)
2. The possibility of exploring super-solar [α/Fe] and super-solar metallicity at the same time is important to break degeneracies in the stellar population parameters and constrain the low-mass end of the IMF slope, especially for massive ETGs. We have enabled this by defining two independent response functions that allow us to extrapolate these SSP models beyond their original parameter spaces, finding remarkable agreement using either of the two functions with their respective SSP model.
3. We find a good agreement with the IMF–$\sigma_\star$ relation obtained in S14 using the extended version of the CvD12 models that allows us to vary age, [α/Fe], IMF, $\Delta T_{\rm eff}$, and [M/H]. However the previously reported trend of a growing deviation of the temperature of the RGB from that predicted by the isochrones with galaxy mass disappears when metallicity is taken as a free parameter, and all σ bins are consistent with $\Delta T_{\rm eff} = -50 \pm 30$.
4. The indices bTiO, TiO_2, CaH_1, and CaT are robust tracers of the IMF slope. Their index strengths give the same predictions for the IMF slope from the extended version of the two models, and there is a minimal dependence on age (at least for old ages), metallicity, and [α/Fe]. TiO_2 plotted as a function of CaH_1 allows us to break the [α/Fe] - IMF degeneracy since the variation of the IMF slope is orthogonal to the [α/Fe] enrichment in this particular plot. However, we note that a zero point offset is present between the EWs of almost all indicators predicted by the two sets of SSP models. Several possible causes for these offsets are investigated in Appendix A but further investigation is required. We nevertheless note that the zero point shifts do not change our main conclusion that the slope of the low-mass end of the IMF is not universal.
5. The situation is more complicated for the indices NaD and NaI. Specifically, the two different models give different predictions for the IMF–$\sigma_\star$ relation when these indices are considered. Observed NaD–NaI values only match CvD12 SSP models with solar metallicity and abundances for ETGs with $\sigma_\star < 250\,{\rm km\,s^{-1}}$, while MIUSCAT models with varying metallicity and solar abundances match the data in all mass bins (Figure 4) but predict an extremely strong variation of the IMF slope, with a maximum of $x = 3.5$ for the most massive mass bin. This result contradicts inferences from the other indices and other published results (Spiniello et al. 2011, 2012, 2014; Cappellari et al. 2012; Conroy & van Dokkum 2012b; Barnabè et al. 2013). We therefore conclude that the use of Na indices to constrain the IMF slope should be carefully examined and treated with caution. Sodium indices should never be used by themselves to constrain the IMF, particularly if one limits oneself to solar-scaled models. NaD is especially affected because it is strongly dependent on [Na/Fe] abundance (at least in CvD12). The strong difference in the NaI index remains unexplained, even when allowing for non-solar Na abundances.

We note that individual elemental abundance variations should be further explored to isolate and test a possible variation of the low-mass end of the IMF slope with galaxy mass. A full-spectrum fitting approach should be the final goal to investigate possible IMF variations with stellar velocity dispersion or other galaxy parameters (such as mass or density) and to disentangle IMF from age, metallicity, and elemental abundances (Conroy et al. 2014). However the approach taken in this paper (and in S14), the first to attempt to compare the two codes fairly, focuses on using specific indices such that one better understands how different parts of the spectrum react to changes in age, metallicity, abundance ratios, effective temperatures and the IMF slope. In addition, it avoids potential issues with flux calibration.

In conclusion, all IMF-sensitive indicators in both models give support to the idea of a non-universality of the low-mass end of the IMF slope, which increases with increasing galaxy mass. Using either CvD12 or MIUSCAT SSP models, a bottom-light IMF such as the Milky Way IMF is inappropriate for the most massive ETGs, as also shown in Spiniello et al. (2012, 2014) and Barnabè et al. (2013). A similar conclusion has been reached in a completely independent way using very different approaches such as dynamics or gravitational lensing analyses (Treu et al. 2010; Cappellari et al. 2012).

We thank Charlie Conroy for providing alternate versions of his models and assistance interpreting them. C.S. thanks Matteo Barnabè, Claudia Maraston, Daniel Thomas, Amina Helmi, Gerjon Mensinga, and Gergo Popping for thoughtful comments that have helped to improve the quality of the manuscript. We thank Michele Cappellari, Sukyuong Ken Yi, and Hyunjin Jeong for interesting discussions and suggestions. Funding for SDSS-III has been provided by the Alfred P. Sloan Foundation, the Participating Institutions, the National Science Foundation, and the U.S. Department of Energy Office of Science. The SDSS-III web site is http://sdss3.org/. SDSS-III is managed by the Astrophysical Research Consortium for the Participating Institutions of the SDSS-III Collaboration including the University of Arizona, the Brazilian Participation Group, Brookhaven National Laboratory, University of Cambridge, Carnegie Mellon University, University of Florida, the

French Participation Group, the German Participation Group, Harvard University, the Instituto de Astrofisica de Canarias, the Michigan State/Notre Dame/JINA Participation Group, Johns Hopkins University, Lawrence Berkeley National Laboratory, Max Planck Institute for Astrophysics, Max Planck Institute for Extraterrestrial Physics, New Mexico State University, New York University, Ohio State University, Pennsylvania State University, University of Portsmouth, Princeton University, the Spanish Participation Group, University of Tokyo, University of Utah, Vanderbilt University, University of Virginia, University of Washington, and Yale University.

APPENDIX A
COMPARING MODEL PREDICTIONS

In this appendix we show how crucial the underlying model assumptions and ingredients, such as stellar libraries or isochrones (especially at high metallicity and for non-solar abundance ratios), are in giving quantitative inferences about the low-mass end of the IMF slope. In fact, although the qualitative trends of the IMF-sensitive features in the two models are similar (both predict an increase (decrease for CaT) in the index strengths from an MW-like to a bottom-heavy IMF), the variation is generally milder for CvD12 and can be very different for certain indices.

The CvD12 and the MIUSCAT models use two different libraries in the optical red and NIR regions (CvD12 uses IRTF; MIUSCAT uses CaT and Indo-US), while in the blue region (3500–7400 Å) they use the same empirical spectral library (MILES). The new set of blue IMF-sensitive indicators defined and used in S14 are therefore essential in this context to eliminate differences arising from the use of different libraries. CvD12 and MIUSCAT predict slightly different variations of indices with IMF slope, even in the wavelength region where they make use of the same empirical spectral library. We investigate the reason for this disagreement and find that one of the largest differences is the use of different isochrones. When using CvD12 models made with the same isochrones used in MIUSCAT models, we find better agreement between the models. However, even when the two sets of models use the same library and the same isochrones, we still find small differences in the predictions of the IMF slopes for some indices. We attribute this to the different methods that the CvD12 and the MIUSCAT models use to attach stars to the isochrones and also to a possible mismatch in the assumed effective temperature of cold stars. Both models test different assumptions for the IMF shape and are created for the specific purpose of examining the stellar content of massive ETGs. They are both mainly based on empirical libraries that generally provide good fits to line strengths and full spectra of populations of solar neighborhood stars. However, empirical stellar libraries are often not able to reproduce consistently the spectral features of systems that have undergone a star formation history (SFH) different than the solar neighborhood. This is, for instance, the case of ellipticals, which have been shown to be overabundant in α-elements with respect to the Sun (e.g., Peterson 1976; Peletier 1989; Worthey et al. 1992). This happens because, by construction, the abundance pattern of models based on empirical libraries is set by the stars in the library, which are mainly observed in the solar neighborhood. On the other hand, a clear advantage of using real stars is that they do not rely on our knowledge of the physics of stellar atmospheres and databases of atomic and molecular transitions.

A.1. Isochrones

An important difference between the models is the set of isochrones used to calculate stellar parameters and spectra. A large number of isochrones exist in the literature (see Conroy 2013 for a review), spanning a wide range of ages and chemical compositions for stars with masses between the hydrogen burning limit ($\sim 0.08\,M_{\odot}$) and $\sim 100\,M_{\odot}$. Different sets of isochrones are tailored for different mass ranges and evolutionary phases of stellar evolution. Some are more effective in tracking the high-mass stars, others focus on the main sequence, RGB, and HB evolution of low-mass stars, such as the Dartmouth models (Dotter et al. 2008). Others are particularly effective at describing the very low-mass end of the IMF down to the brown dwarf regime, such as the Lyon models (Chabrier & Baraffe 1997; Baraffe et al. 1998). Since no single set of available isochrones covers a full range of ages, metallicity, and evolutionary phases, most stellar population synthesis models use a combination of different isochrones. Combining various sets of isochrones is not trivial because different stellar interior models can make different physical assumptions (convection, rotation, etc.), and consequently the age at which stars evolve away from the main sequence can vary between models.

Commonly used isochrones for the bulk of the age and metallicity range of elliptical galaxies include the Padova isochrones (Bertelli et al. 1994; Girardi et al. 2000; Marigo et al. 2008) and the BaSTI models (Pietrinferni et al. 2004; Cordier et al. 2007). These are often supplemented with the Geneva models (Schaller et al. 1992; Meynet & Maeder 2000) at younger ages. Little attention has been paid in the past to the lowest-mass portion of the isochrones, since low-mass stars contribute only a few percent of the light of an old stellar population in the optical (e.g., Worthey 1994; Renzini 2006; Conroy 2013). However, if one wants to study the low-mass end slope of the IMF, this 1–5% contribution is crucial. It is for this reason that CvD12 decided to use the Lyon models for stars with masses below $0.2\,M_{\odot}$. The Lyon models use the surface boundary condition of the base of the atmosphere (rather than at $T = T_{\rm eff}$), which is better for stellar interior codes that are not ideally suited to compute the physical conditions for high-density, low-temperature environments down to $T = T_{\rm eff}$ (CvD12). Using only the solar-scaled theoretical Padova isochrones of Girardi et al. (2000), the MIUSCAT library cuts off at $0.15\,M_{\odot}$, since the Padova isochrones do not extend to lower masses.

The CvD12 models allow a more accurate treatment of the low-mass stars down to the hydrogen burning limit ($M_{\rm low} = 0.08\,M_{\odot}$), using several separate evolutionary calculations (a combined set of different isochrones and empirical and theoretical libraries) and adding the SDSS dM stellar templates of Bochanski et al. (2007) to the MILES library.

In Figure 3 an offset between the EWs of TiO lines predicted from MIUSCAT and CvD12 models with the same parameters is found. To investigate the origin of this offset and to test the importance of isochrones in constraining the IMF slope from TiO indices, Prof. Conroy kindly built and provided us with new CvD12 models using Padova isochrones for all stellar evolutionary phases.

In Figure 6 we show the response of the EWs of IMF-sensitive features to the variation of the low-mass end of the IMF slope for the publicly available versions of MIUSCAT (red solid line) and CvD12 (black solid) SSP models with the

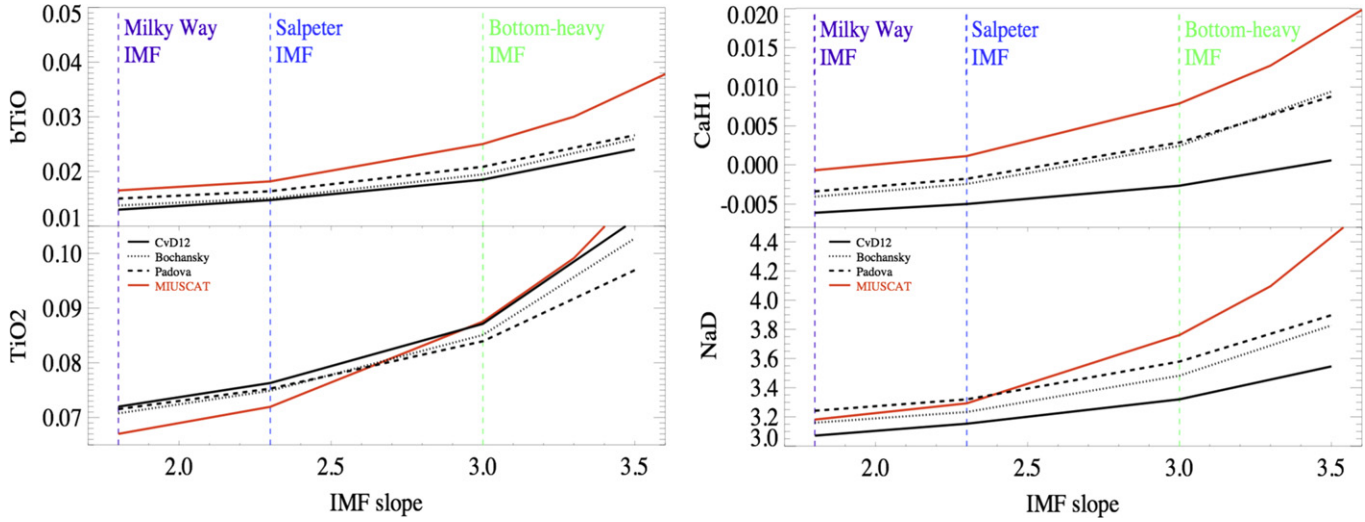

Figure 6. Variation of bTiO, TiO_2, CaH_1, and NaD indices with IMF slope. Black solid lines are a CvD12 SSP model of 12.5 Gyr built using a different set of isochrones for the different stellar evolutionary phases. Black dotted lines are the same models with the addition of the SDSS dM stellar templates of Bochanski et al. (2007) to augment the number of M dwarfs. Black dashed lines are CvD12 SSP models built using the Padova isochrones (see the caption and text for more details). Red lines are MIUSCAT SSP models with the same age. Vertical colored lines show different IMFs.

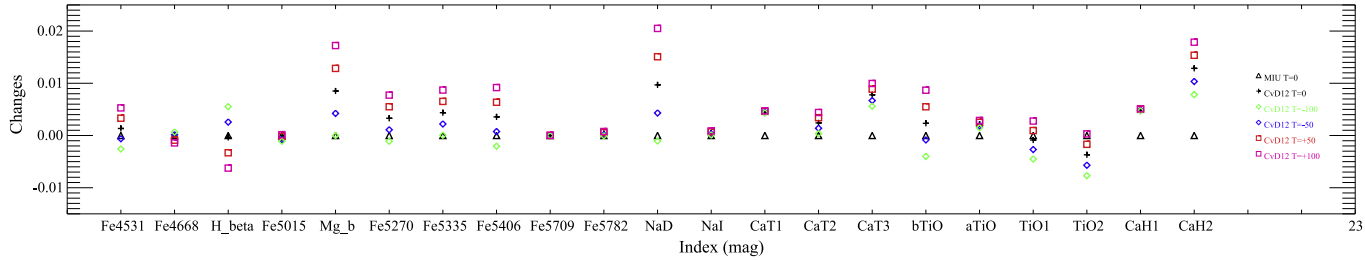

Figure 7. Variation of EWs (measured in mag) for CvD12 models with 12.5 Gyr, Salpeter IMF, solar abundance patterns, and varying $T_{\rm eff}$ (different colors, see the caption) with respect to the EW of a MIUSCAT model with the same parameters and $T_{\rm eff} = 0$ (black triangle, set to zero value).

same age, solar [α/Fe], and metallicity, and for the modified CvD12 models with Padova isochrones (dashed black line). We also plot a CvD12 model with the same age and metallicity obtained with the addition of the SDSS dM stellar templates of Bochanski et al. (2007; dotted line). Because CvD12 and MIUSCAT make use of the same empirical stellar library (MILES) in this spectral region the main difference between the two sets of models is the assumed isochrones. Although the predictions of the two SSP models agree qualitatively, the MIUSCAT models suggest a steeper variation of all the indices with IMF slope, which affects the IMF–$\sigma^{\star}$ relation. For all indices except TiO_2, the discrepancy between MIUSCAT and CvD12 becomes smaller when the two models make use of the same stellar isochrones, as expected.

However, in the particular case of the TiO_2 index, the models do not predict the same variation of the indices with IMF slope, even when they make use of the same empirical stellar library and set of isochrones, and actually the CvD-Padova models are in even worse agreement with MIUSCAT Padova-based models. Consequently, we argue that this difference must arise from a different cause. One possibility is the different methods used in the CvD12 and MIUSCAT models to attach stars to the isochrones at low mass. The MIUSCAT models obtain stellar fluxes from the theoretical parameters of the isochrones ($T_{\rm eff}$, log g, [Z/H]) using empirical relations between colors and stellar parameters (temperature, gravity, and metallicity, respectively). Their algorithm, described in Vazdekis et al. (2003, 2010), finds the closest stars and weights them according to the distance to the target point ($T_{\rm eff,0}$, log g_0, $[{\rm Fe/H}]_0$) in the stellar parameter space. The CvD12 SSP models use instead a M–$L_{\rm bol}$ relation, choose the closest observed stellar spectrum from the IRTF library with the appropriate bolometric luminosity, and then match it to a MILES spectrum at shorter wavelengths. For instance, this different interpolation scheme and the different physical approach could cause a zero point shift in the assumed effective temperature of the stars used in the SSP models. We further discuss this point in the next section, although we do not have the possibility to investigate this in detail.

A.2. Effective Temperature

We have made an attempt to understand the origin of the zero point differences of index strengths between the two SSP models by changing the temperature of the isochrones as described by Conroy & van Dokkum (2012a, 2012b), in which the effective temperatures of all stars along an isochrone are shifted by an amount within the observational and systematic uncertainties in the effective temperature scale of normal giants and dwarfs (roughly $\pm$100 K). There are currently no public versions of the MIUSCAT models that include such a shift, so we have shifted the effective temperatures of a solar abundance, 12.5 Gyr old, Salpeter IMF CvD12 model by up

to ±100 K and compared them with the same MIUSCAT model.[9] We plot the results in Figure 7, where we have converted indices in Å to magnitudes using the conversion given by Kuntschner (2000, his Equation (2)) for easy comparison. We find that there is no consistent shift that brings all indices into agreement between the models, and for some indices (namely CaT1, CaT3, and the two CaH indices) there is no reasonable temperature shift able to bring the two models into agreement. Without having the ability to change the temperature of stars independently along the isochrones, we cannot proceed further with this analysis. We merely point out here that these zero point differences likely arise from the different $T_{\rm eff}$–$M_{\rm bol}$ relations, i.e., the different methods of attaching stellar spectra to isochrones assumed by the two models and possibly by the different spectral libraries used redward of 7500 Å.

A.3. Index Variation Comparisons

To compare predictions from the two models, we calculate index variations as a function of the IMF slope and the age of several optical indices for both the MIUSCAT and CvD12 models. In Figure 8, we show the predicted index variations for a range of CvD12 models (upper panels) and MIUSCAT models (lower panels) with different ages (lines of different colors). Here we restrict our comparison to solar abundances and metallicity (using only the publicly available set of models), because here in the appendix we do not compare the SSP models with massive (metal-rich and α-enhanced) ETGs. We also restrict the comparison to the unimodal IMF case, the only one explored by CvD12.

Figure 8 confirms that most of the blue classical Lick indices (Burstein et al. 1984; Worthey 1994; Trager et al. 1998) do not depend (or depend only weakly) on the IMF slope, while the Na, TiO, and CaH indices increase from MW IMF to a bottom-heavy IMF for both models (as already shown in S14). The only IMF-sensitive index that grows weaker with increasing IMF slope is CaT, as seen in previous studies (e.g., Cenarro et al. 2003; Conroy & van Dokkum 2012a).

For the majority of the indices, the gradient of the variation is similar, although generally slightly milder for the CvD12 models than for the MIUSCAT models. For some indices, however, the two SSP models give quite different predictions for IMF variations. CaH_1 is an extreme case, and in addition bTiO and both the sodium indices (NaI and NaD) behave differently in the two sets of models. We further investigate the behavior of these particular indices in the following sections. Predictions for the Hβ index are also different, although this index depends only weakly on the IMF slope. In fact, for the MIUSCAT models the Hβ decreases with increasing IMF slope, whereas it remains nearly constant for CvD12 models. Because this index is mainly (but not entirely: see Worthey 1994) contributed by turn-off stars at solar metallicity (Buzzoni et al. 1994), its sensitivity to the IMF slope must be understood as a relative change of the contributing fraction of such hot stars.

On the other hand, index variations with an IMF slope of the redder TiO features predicted from the two SSP models are similar, and variations of CaH_2 and CaT are also similar. However, for these indicators, the trends of the variation of EWs with age reverse for the youngest ages. A possible explanation for this could be the presence of a more extended AGB contribution in the CvD12 models with respect to the MIUSCAT models.

Moreover, for some indices, there is also a shift in the zero point: for the MW IMF, the NaD indices of the CvD12 models with solar abundance are systematically lower than the MIUSCAT models, while the TiO_1 and TiO_2 indices are systematically higher. Small differences in the metallicity-sensitive features could be due to the different ways the two sets of models deal with metallicity and/or [α/Fe]. This will be addressed in the following section.

To further quantify the differences between the variation with IMF predicted on a single index from the two sets of SSP models we compute the following quantities,

$$\Delta\mathrm{IMF} = I_{i,(x=3.5)} - I_{i,(\mathrm{MW})} \quad (6)$$

$$\Delta\mathrm{IMF}_{\mathrm{Salp}} = I_{i,(x=3.5)} - I_{i,(\mathrm{Salp})} \quad (7)$$

$$\Delta\mathrm{IMF}_{\mathrm{MW}} = I_{i,(\mathrm{Salp})} - I_{i,(\mathrm{MW})} \quad (8)$$

for the index i, in an old model with an age of ∼13.5 Gyr for CvD12 and ∼14.1 Gyr for MIUSCAT. The first equation measures the variation of the index i with an IMF slope from the MW IMF to an extremely bottom-heavy IMF (slope of $x = 3.5$), while the second and the third measure the variation of the index i with an IMF slope from a Salpeter to $x = 3.5$ and from an MW IMF to a Salpeter IMF, respectively.

In Table 1 we report the values of the three ΔIMFs for the selected indices, separated by the units in which they are computed. We also report between parentheses the fractional changes (for indices in Å, these are calculated by normalizing each quantity with respect to the lower-slope value; for magnitude indices, we use the approximation that for small changes, i.e., <25%, magnitude differences are nearly the same as percentage changes).

A good qualitative agreement is found between the two sets of models for some of the indices, although the MIUSCAT models typically predict a larger variation of EW with IMF slope. This result also confirms the existence of the IMF–$\sigma_\star$ relation given in Spiniello et al. (2014).

By comparing the curves in Figure 8 with the entries in Table 1, we can further understand the differences in the index variations of the two models. For instance, in the CvD12 models, Hβ does not depend at all on IMF (only ∼2% variation from the MW IMF to $x = 3.5$), while the MIUSCAT models predict a (mild) anti-correlation of the EW of Hβ with a fractional change of the EW of 10%.

TiO and CaH indices behave similarly in the two models, but MIUSCAT predicts overall steeper variations, especially for very bottom-heavy IMFs. The CaT index shows an anti-correlation of the EW with the IMF slope for both models.

The values of the variations predicted by CvD12 for the NaI and NaD indices are instead very different in all the ΔIMF ranges than the values predicted for the same features by MIUSCAT, even though the values for an MW-like IMF are similar between the models (i.e., no zero point shift is present in the case of sodium).

APPENDIX B
THE [Na/Fe] ABUNDANCE PATTERN FROM CVD12

In Section 3 we conclude that both the CvD12 and MIUSCAT extended versions of the models suggest a non-

[9] The effective temperature difference vector for $\lambda > 4500$ Å was kindly provided by Dr. Conroy.

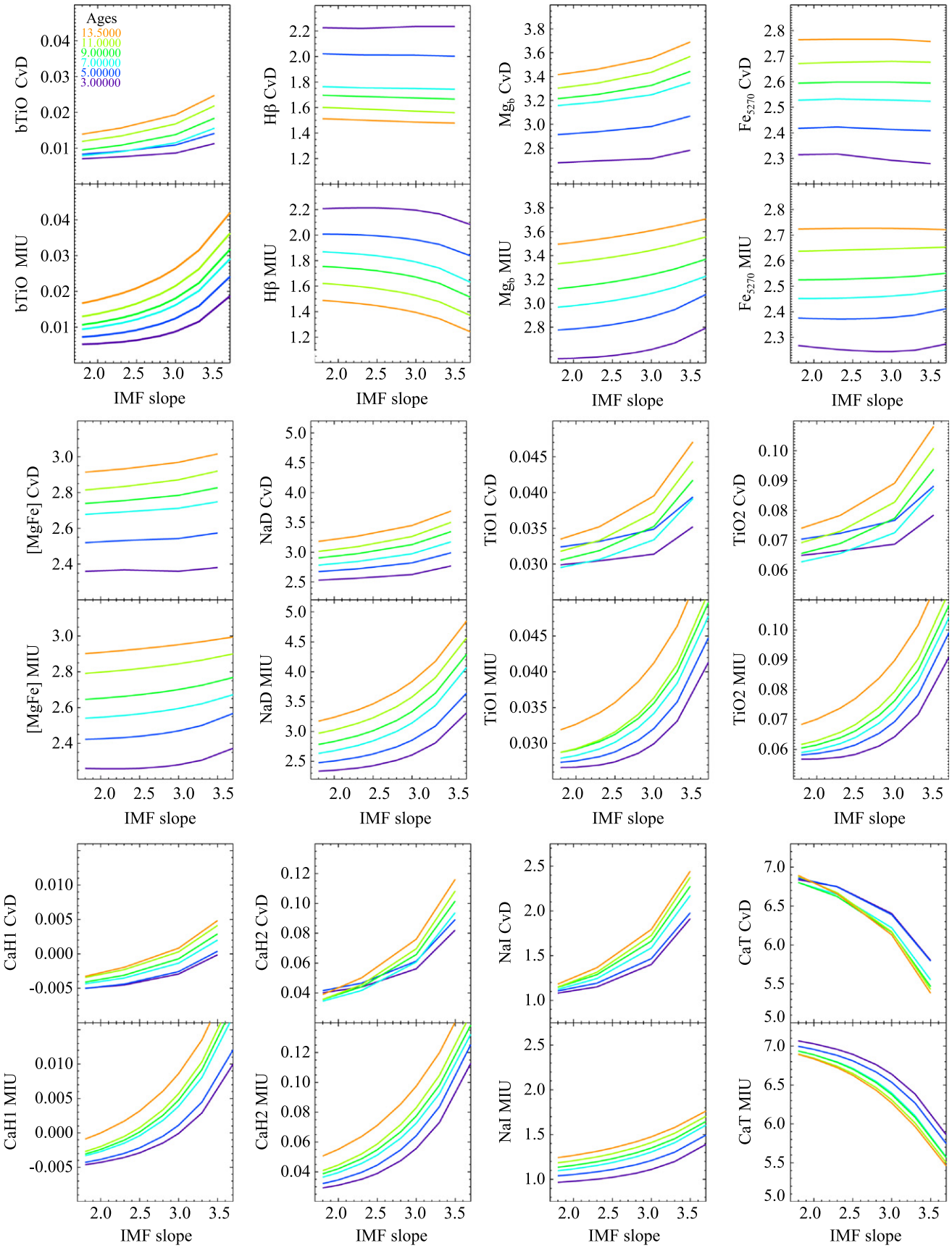

Figure 8. Variation of index strengths with IMF slope predicted for the CvD12 models (upper panels) and the MIUSCAT models (lower panels), convolved to a common resolution of $\sigma = 350$ km s^{-1}. In each panel, different colors represent SSP models with different ages, as indicated in the legend on the first panel. TiO and CaH indices are given in magnitudes, while all the other indices are given in Å. Note here that the MW IMF results are given at an IMF slope of $x = 1.8$ for convenience.

Table 1
ΔIMF for the Selected Indices Predicted from the Two SSP Models

Index (mag)	EW_{Salp} CvD12	EW_{Salp} MIUSCAT	ΔIMF CvD12	ΔIMF MIUSCAT	ΔIMF_{Salp} CvD12	ΔIMF_{Salp} MIUSCAT	ΔIMF_{MW} CvD12	ΔIMF_{MW} MIUSCAT
bTiO	0.016	0.019	0.011(1.1%)	0.026(2.6%)	0.009(0.9%)	0.023(2.3%)	0.002(0.2%)	0.003(0.3%)
TiO_1	0.035	0.034	0.014(1.4%)	0.017(1.7%)	0.012(1.2%)	0.015(1.5%)	0.002(0.2%)	0.002(0.2%)
TiO_2	0.078	0.074	0.034(3.4%)	0.048(4.8%)	0.030(3.0%)	0.042(4.2%)	0.004(0.4%)	0.005(0.5%)
CaH_1	−0.0019	0.0017	0.008(0.8%)	0.020(2.0%)	0.006(0.6%)	0.018(1.8%)	0.001(0.1%)	0.003(0.3%)
CaH_2	0.050	0.064	0.077(7.7%)	0.095(9.5%)	0.066(6.6%)	0.082(8.2%)	0.011(1.1%)	0.001(0.1%)
Index (Å)	EW_{Salp} CvD12	EW_{Salp} MIUSCAT	ΔIMF CvD12	ΔIMF MIUSCAT	ΔIMF_{Salp} CvD12	ΔIMF_{Salp} MIUSCAT	ΔIMF_{MW} CvD12	ΔIMF_{MW} MIUSCAT
Hβ	1.502	1.461	−0.034(2.3%)	−0.14(9.6%)	−0.024(1.6%)	−0.116(8%)	−0.011(0.7%)	−0.027(1.8%)
Mgb	3.460	3.535	0.274(8.0%)	0.153(4.4%)	0.230(6.6%)	0.113(3.2%)	0.044(1.3%)	0.040(1.1%)
Fe5270	2.766	2.726	−0.007(0.2%)	0.001(0.05%)	−0.009(0.3%)	−0.001(0.05%)	0.002(0.07%)	0.003(0.1%)
MgFe	2.932	2.919	0.102(3.5%)	0.067(2.3%)	0.083(2.8%)	0.049(1.7%)	0.018(0.6%)	0.018(0.6%)
NaD	3.268	3.359	0.507(16%)	1.00(31%)	0.42(13%)	0.816(24%)	0.087(2.8%)	0.185(5.8%)
NaI	1.365	1.313	1.26(100%)	0.337(27%)	1.079(79%)	0.267(20%)	0.182(15%)	0.070(5.6%)
CaT	6.655	6.723	−1.514(19%)	−0.926(13%)	−1.28(17%)	−0.757(11%)	−0.238(3%)	−0.17(2.5%)

Note. Indices are separated by the units in which they are computed. We report as reference the value of the indices for a model with a Salpeter IMF. These values are useful to highlight zero point differences in the two sets of models. We report the percentage change compared to the EW for the lower slope IMF in each case between parentheses.

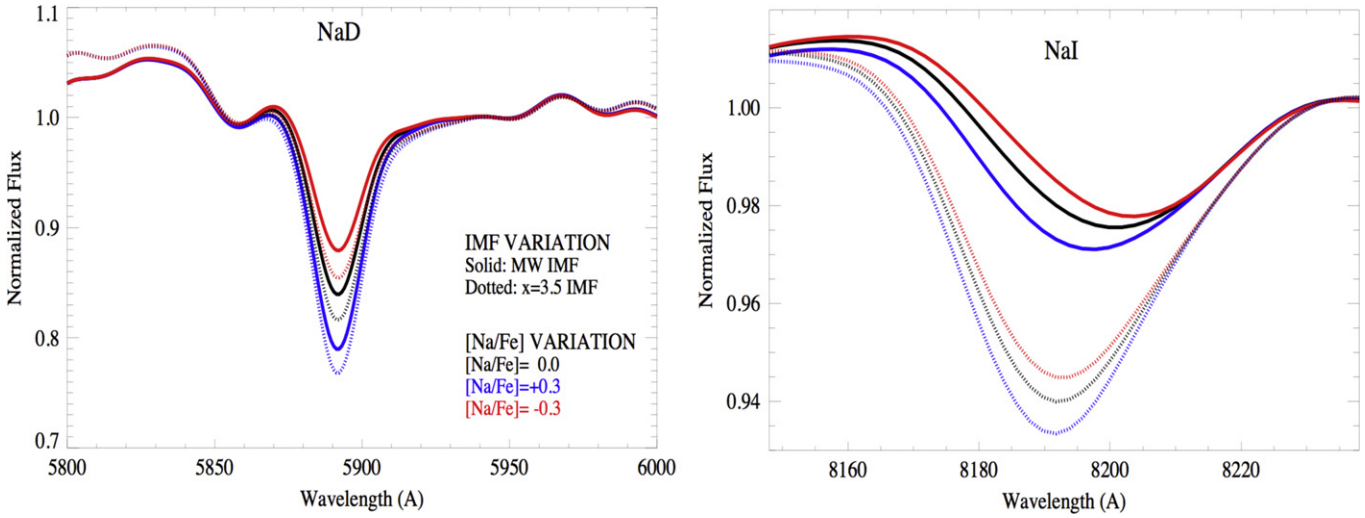

Figure 9. Spectra of a CvD12 model with an age of 13.5 Gyr in the regions of the NaD (left) and NaI (right) features. Different colors are models with different [Na/Fe] abundances (between −0.3 and +0.3), solid lines are models with MW IMF, and dotted lines represent models with an extremely bottom-heavy IMF ($x = 3.5$). NaD is more sensitive to abundance variations than to IMF, whereas NaI is much more sensitive to variations in the IMF slope. Because the MIUSCAT models only have the solar abundance pattern, we cannot repeat this test for those models.

universal IMF whose low-mass end steepens with the velocity dispersion for the averaged SDSS ETGs. This result clearly shows that the dependence of the low-mass end of the IMF ($\leqslant 0.3\,M_{\odot}$) on the stellar velocity dispersion (stellar mass) of the system (e.g., Auger et al. 2010; Napolitano et al. 2010; Treu et al. 2010; van Dokkum & Conroy 2010; Spiniello et al. 2011, 2012, 2014) is genuine and does not arise from any misunderstanding of the ingredients of the SSP models.

However, we also demonstrated that the two different models give different predictions for the IMF–$\sigma_{\star}$ relation when sodium indices are considered. Observed NaD–NaI values only match CvD12 SSP models with solar metallicity and abundances for ETGs with $\sigma_{\star} < 250\,\mathrm{km\,s^{-1}}$, while MIUSCAT models with varying metallicity and solar abundances match the data in all mass bins (Figure 4(a)), but predict an extremely strong variation of the IMF slope with a maximum of $x = 3.5$ for the most massive mass bin (and moreover they fail to reproduce the NaD–CaH_1 EWs at all sigmas). Here we focus on this issue. We use the CvD12 models, the only current SSP allowing for a non-solar sodium abundance pattern, to decouple the IMF variations from the abundance variations for each of the two sodium lines. Using the CvD12 models with different [Na/Fe] abundances, we study the behavior of the NaD and the NaI indices when varying the IMF slopes at a fixed sodium abundance and when varying [Na/Fe] at a fixed IMF slope. In Figure 9 we show the CvD12 models with an age of 13.5 Gyr, zooming in on the regions of the NaD (left panel) and NaI (right panel) features. In both panels different colors show models with different [Na/Fe], from −0.3 to +0.3, while different linestyles represent models with different IMF slopes,

Table 2
Ratio Between the Fractional Changes in Indices with an IMF Slope and with Sodium Abundances at a Fixed Age, Predicted by the CvD12 SSP Models

Index	ΔIMF/Δ[Na/Fe]
NaD	0.29
NaI	4.21

from the MW IMF to 3.5. The figure clearly demonstrates that NaD absorption is more sensitive to [Na/Fe] than the redder NaI feature, which varies much more with the IMF slope.

This sensitivity can be quantitatively expressed as

$$\left(\frac{\Delta \mathrm{IMF}}{\Delta[\mathrm{Na/Fe}]}\right)_i = \frac{I_{i,(x=3.5)[\mathrm{Na/Fe}]=0} - I_{i,(\mathrm{MW})[\mathrm{Na/Fe}]=0}}{\left\langle I_{i,([\mathrm{Na/Fe}]=+0.3)} - I_{i,([\mathrm{Na/Fe}]=-0.3)} \right\rangle_{x=[\mathrm{MW}-3.5]}} \quad (9)$$

for both indices (see Table 2). In this equation, the numerator measures the variation of an index i with IMF slope from a Milky Way-like IMF to an extremely bottom-heavy IMF (slope of $x = 3.5$), while the denominator is the average of the index variation with sodium abundances in the range $[\mathrm{Na/Fe}] = [-0.3, +0.3]$ for the two IMFs.

The larger the value of ΔIMF/Δ[Na/Fe],the larger the sensitivity to IMF slope compared with the sensitivity to Na abundance. NaI is ~4 times more sensitive to variations in IMF slope than to variations in sodium abundances, whereas NaD is ~3 times more sensitive to [Na/Fe] than to IMF slope.

Thus a non-solar [Na/Fe] abundance in massive galaxies could explain the fact that in panel (a) of Figure 4 CvD12 models with solar abundances only match the low-mass systems. As highlighted by Conroy & van Dokkum (2012a, 2012b) and by S12, more massive ETGs require a higher [Na/Fe] and a steep (Salpeter or slightly steeper) IMF slope. The IMF slopes inferred from MIUSCAT models from panel (a) appear to be steeper probably because the change in the NaD EWs is attributed completely to IMF variations, as the models have solar [Na/Fe] abundance. NaD is especially affected in this context because it is strongly dependent on [Na/Fe] abundance (~4 times more than the redder NaI). The strong disagreement between the models regarding the NaI index, which is less affected in this context, remains unexplained.

Hence, we conclude that the use of Na indices in constraining the IMF slope should be more carefully examined and considered with caution. In particular, they should never be used by themselves to constrain the IMF, if one limits oneself to solar-scaled models.

REFERENCES

Alexander, D. R., & Ferguson, J. W. 1994, ApJ, 437, 879
Alloin, D., & Bica, E. 1989, A&A, 217, 57
Arrigoni, M., Trager, S. C., Somerville, R. S., & Gibson, B. K. 2010, MNRAS, 402, 173
Auger, M. W., Treu, T., Gavazzi, R., et al. 2010, ApJL, 721, L163
Baraffe, I., Chabrier, G., Allard, F., & Hauschildt, P. H. 1998, A&A, 337, 403
Barnabè, M., Spiniello, C., Koopmans, L. V. E., et al. 2013, MNRAS, 436, 253
Bastian, N., Covey, K. R., & Meyer, M. R. 2010, ARA&A, 48, 339
Bell, E. F., & de Jong, R. S. 2001, ApJ, 550, 212
Bertelli, G., Bressan, A., Chiosi, C., Fagotto, F., & Nasi, E. 1994, A&AS, 106, 275
Bochanski, J. J., West, A. A., Hawley, S. L., & Covey, K. R. 2007, AJ, 133, 531
Bressan, A., Chiosi, C., & Fagotto, F. 1994, ApJS, 94, 63
Bruzual, G., & Charlot, S. 1993, ApJ, 405, 538
Bruzual, G., & Charlot, S. 2003, MNRAS, 344, 1000
Burstein, D., Faber, S. M., Gaskell, C. M., & Krumm, N. 1984, ApJ, 287, 586
Buzzoni, A. 1989, ApJS, 71, 817
Buzzoni, A., Mantegazza, L., & Gariboldi, G. 1994, AJ, 107, 513
Cappellari, M., McDermid, R. M., Alatalo, K., et al. 2012, Natur, 484 485
Carter, D., Visvanathan, N., & Pickles, A. J. 1986, ApJ, 311, 637
Cenarro, A. J., Cardiel, N., Gorgas, J., et al. 2001, MNRAS, 326, 959
Cenarro, A. J., Gorgas, J., Vazdekis, A., Cardiel, N., & Peletier, R. F. 2003, MNRAS, 339, L12
Chabrier, G. 2003, PASP, 115, 763
Chabrier, G. 2005, in The Initial Mass Function 50 Years Later, Vol. 327, ed. E. Corbelli, F. Palla, & H. Zinnecker (Dordrecht: Springer), 41
Chabrier, G., & Baraffe, I. 1997, A&A, 327, 1039
Choi, J., Conroy, C., Moustakas, J., et al. 2014, ApJ, 792, 95
Conroy, C. 2013, ARA&A, 51, 393
Conroy, C., Graves, G., & van Dokkum, P. 2014, ApJ, 780, 33
Conroy, C., & van Dokkum, P. 2012a, ApJ, 747, 69
Conroy, C., & van Dokkum, P. G. 2012b, ApJ, 760, 71
Cordier, D., Pietrinferni, A., Cassisi, S., & Salaris, M. 2007, AJ, 133, 468
Cushing, M. C., Rayner, J. T., & Vacca, W. D. 2005, ApJ, 623, 1115
Dotter, A., Chaboyer, B., Jevremović, D., et al. 2008, ApJS, 178, 89
Ferreras, I., la Barbera, F., de la Rosa, I. G., et al. 2013, MNRAS, 429, L15
Girardi, L., Bressan, A., Bertelli, G., & Chiosi, C. 2000, A&AS, 141, 371
González, J. J. 1993, PhD thesis, Univ. California
Jeong, H., Yi, S. K., Kyeong, J., et al. 2013, ApJS, 208, 7
Kroupa, P. 2001, MNRAS, 322, 231
Kuntschner, H. 2000, MNRAS, 315, 184
La Barbera, F., Ferreras, I., Vazdekis, A., et al. 2013, MNRAS, 433, 3017
Läsker, R., van den Bosch, R. C. E., van de Ven, G., et al. 2013, MNRAS, 434, L31
Leitherer, C., Schaerer, D., Goldader, J. D., et al. 1999, ApJS, 123, 3
Maraston, C. 2005, MNRAS, 362, 799
Marigo, P., Girardi, L., Bressan, A., et al. 2008, A&A, 482, 883
Meynet, G., & Maeder, A. 2000, A&A, 361, 101
Napolitano, N. R., Romanowsky, A. J., & Tortora, C. 2010, MNRAS, 405, 2351
O'Connell, R. W. 1976, ApJ, 206, 370
Peletier, R. F. 1989, PhD thesis, Univ. Groningen
Peterson, R. C. 1976, ApJL, 210, L123
Pietrinferni, A., Cassisi, S., Salaris, M., & Castelli, F. 2004, ApJ, 612, 168
Renzini, A. 2006, ARA&A, 44, 141
Salpeter, E. E. 1955, ApJ, 121, 161
Sánchez-Blázquez, P., Peletier, R. F., Jiménez-Vincente, J., et al. 2006, MNRAS, 371, 703
Schaller, G., Schaerer, D., Meynet, G., & Maeder, A. 1992, A&AS, 96, 269
Spiniello, C., Koopmans, L. V. E., Trager, S. C., Czoske, O., & Treu, T. 2011, MNRAS, 417, 3000
Spiniello, C., Trager, S., Koopmans, L. V. E., & Conroy, C. 2014, MNRAS, 438, 1483
Spiniello, C., Trager, S. C., Koopmans, L. V. E., & Chen, Y. P. 2012, ApJL, 753, L32
Tinsley, B. M. 1968, ApJ, 151, 547
Tinsley, B. M. 1972, ApJ, 178, 319
Tinsley, B. M., & Gunn, J. E. 1976, ApJ, 206, 525
Tortora, C., Romanowsky, A. J., & Napolitano, N. R. 2013, ApJ, 765, 8
Trager, S. C., Faber, S. M., & Dressler, A. 2008, MNRAS, 386, 715
Trager, S. C., Faber, S. M., Worthey, G., & González, J. J. 2000a, AJ, 120, 165
Trager, S. C., Faber, S. M., Worthey, G., & González, J. J. 2000b, AJ, 119, 1645
Trager, S. C., Worthey, G., Faber, S. M., Burstein, D., & Gonzalez, J. J. 1998, ApJS, 116, 1
Treu, T., Auger, M. W., Koopmans, L. V. E., et al. 2010, ApJ, 709, 1195
Valdes, F., Gupta, R., Rose, J. A., Singh, H. P., & Bell, D. J. 2004, ApJS, 152, 251
van Dokkum, P. G., & Conroy, C. 2010, Natur, 468, 940
Vazdekis, A., Casuso, E., Peletier, R. F., & Beckman, J. E. 1996, ApJS, 106, 307
Vazdekis, A., Cenarro, A. J., Gorgas, J., Cardiel, N., & Peletier, R. F. 2003, MNRAS, 340, 1317

Vazdekis, A., Ricciardelli, E., Cenarro, A. J., et al. 2012, MNRAS, 424, 157
Vazdekis, A., Sánchez-Blázquez, P., Falcón-Barroso, J., et al. 2010, MNRAS, 404, 1639
Worthey, G. 1992, Ph.D. Thesis, California Univ., Santa Cruz
Worthey, G. 1994, ApJS, 95, 107
Worthey, G. 1998, PASP, 110, 888
Worthey, G., Faber, S. M., & Gonzalez, J. J. 1992, ApJ, 398, 69
Worthey, G., Ingermann, B. A., & Serven, J. 2011, ApJ, 729, 148